University of Sistan and Baluchestan

Challenges in Nano and Micro Scale Science and Technology

Online ISSN: 2821 - 000X

Fabrication and Modeling of a Polymeric Triboelectric Nanogenerator Considering the Edge-Effect Capacitor

Mohsen Keykha[1] | Tahereh Fanaei Sheikholeslami[2]✉ | Amin Behzadmehr[3]

1. Department of Electrical Engineering, University of Sistan and Baluchestan, Zahedan, I.R. Iran
2. Corresponding Author, Department of Mechanical Engineering, University of Sistan and Baluchestan, Zahedan, I.R. Iran. Email: tahere.fanaei@ece.usb.ac.ir
3. Department of Mechanical Engineering, University of Sistan and Baluchestan, Zahedan, I.R. Iran

Article Info

Article type:
Research Article

Keywords:
TENG,
Impact force,
environmental motions,
KAPTON,
PDMS

ABSTRACT

A vertical two-electrode polymeric nanogenerator energy harvester, utilizing KAPTON and PDMS as the positive and negative triboelectric materials, respectively, was investigated through both experimental and numerical approaches. To simulate environmental low-frequency motions, a vibrational force of 20 mN at 8 Hz was applied to the device using a custom-designed mechanical instrument. Experimental measurements confirmed the nanogenerator's ability to generate an output voltage and current with maximum amplitudes of 4 V and 0.025 μA, respectively. The charge production mechanism of the device was then modeled numerically, both with and without the inclusion of the edge-effect capacitor. The modeling results demonstrated strong agreement with experimental data, with the incorporation of the edge-effect capacitor significantly improving the alignment between calculated and observed values. The validated model provides a valuable tool for designing high-performance triboelectric nanogenerators for various applications and conditions. Additionally, further investigations into environmental influences revealed reduced device performance at lower pressures and higher temperatures.

INTRODUCTION

The transition to renewable and clean energy sources represents a crucial solution to mitigate the depletion of fossil fuels and their detrimental environmental impacts. Among alternative energy sources, mechanical vibrations and random environmental movements offer promising potential due to their ubiquitous presence in daily life [1,2]. Recent research has investigated intrinsic material properties such as piezoelectricity, electromagnetism, thermoelectricity, and triboelectricity to facilitate the conversion of mechanical energy into electrical energy. These properties are utilized in specifically designed devices, including nano- and micro-scale generators [3,4]. Nanogenerators have found application in self-powered sensors, actuators, and wireless microelectronic systems.

Triboelectric nanogenerators (TENGs), which operate based on electron transport facilitated by the triboelectric effect between two distinct materials [5], have garnered significant attention due to their material-dependent performance characteristics. Polymeric materials such as KAPTON, PVC, PET, and PDMS have been widely employed in TENG fabrication, with studies indicating that KAPTON-PET pairs outperform PVC-PET pairs in energy output [6].

Innovations in TENG development have further expanded their functional capabilities. For instance, Niu et al. [7] fabricated a self-healing triboelectric nanogenerator using Ag nanowires embedded within a soft polymer matrix, achieving exceptional stability and flexibility. Mull et al. [8] demonstrated robust operational durability with a single-electrode-mode TENG utilizing polypyrrole-coated cotton textiles, even under extended cyclic contact-separation conditions. Shao et al. [9] introduced a theoretical model for TENGs based on Maxwell's equations, presenting them as lumped circuit elements suitable for low-frequency operation.

Chen et al. [10] constructed TENGs using chitosan-silk fibroin-airlaid (CAS) paper composite films, achieving high energy harvesting efficiency. Heydari et al. [11,12] developed and optimized a zero-inductance spiral electrode TENG capable of generating electricity irrespective of motion direction. Their findings also demonstrated its viability as a Zero Power dynamic sensor.

Comprehensive theoretical models for TENGs, incorporating mathematical, physical, electromechanical,

How to Cite this paper: Keykha M., Fanaei Sheikholeslami T., Behzadmehr A. Fabrication and Modeling of a Polymeric Triboelectric Nanogenerator Considering the Edge-Effect Capacitor. *Challenges in Nano and Micro Scale Science and Technology*. 2024; 12(1): 19-26. DOI: 10.22111/cnmst.2025.51742.1260

© Keykha M., Fanaei Sheikholeslami T., Behzadmehr A. Publisher: University of Sistan and Baluchestan.

DOI: 10.22111/cnmst.2025.51742.1260

and circuit-based frameworks, were presented by Shao et al. [13]. Sun et al. [14] extended these analyses by introducing dynamic models accounting for both mechanical and electrical systems, proposing optimal execution strategies to maximize energy output. Zhao et al. [15] validated a systematic theoretical approach for contact-separation mode TENGs and proposed a universal electrodynamic model applicable to TENGs of varying dimensions.

While variable capacitors are commonly employed to model TENGs and extract governing equations [16-18], additional capacitive and non-capacitive elements influencing performance have often been overlooked. In the present study, a triboelectric nanogenerator was fabricated using KAPTON-PDMS polymer pairs, and its performance was analyzed both experimentally and theoretically. The model was refined by incorporating edge capacitors to improve accuracy. Furthermore, the effects of parameters such as air gap variations, device capacitance changes, and environmental conditions on TENG performance were systematically investigated.

Experimental Procedure

Materials and Design

A nanogenerator with the structure of metal/KAPTON/Air/PDMS/metal was designed and fabricated. The proposed structure schematically illustrated in Fig. 1. The device features a cross-sectional area (S) of 2 × 2 cm² (W=l=2 cm), with aluminum and copper employed as top and bottom metal electrodes, 1 and 2, respectively, with a thickness of about 120 μm for each electrode. Table 1 provides the dimensions and key properties of the polymeric materials utilized in the device.

Table 1
Material properties and structural parameters of the triboelectric nanogenerator

Materials and properties	MAT 1: KAPTON	MAT 2: PDMS [19]
Dielectric coefficient	3.4	2.5
Density (g/cm^3)	1.42	0.97
Tensile strength (MPa)	231	2.23
Thicknesses (d_1,d_2) (μm)	60	100
Pressure (torr)	760	
Temperature (°C)	20	

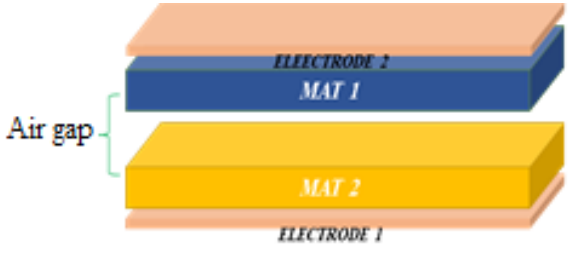


Fig. 1. Schematic of the vertical two electrode triboelectric nanogenerator

To fabricate the proposed TENG, a PDMS film featuring a pyramidal structure was synthesized to enhance electron loss from the material via the sharp points at the apex of the pattern. The PDMS liquid and curing agent were mixed at a 1:10 ratio to achieve the desired composition. To ensure uniformity and homogeneity, bubbles within the mixture were eliminated by subjecting it to vacuum conditions for 1 hour. The gel-like mixture was subsequently poured into a mold with a pyramidal pattern and cured in a furnace at 80°C for 1 hour. Once cured, the pyramidal-patterned PDMS film was carefully peeled off from the mold. The film was then attached to the aluminum electrode using silver adhesive, forming the lower layer of the TENG, as depicted in Fig. 2. For the upper layer, film of KAPTON was attached to the copper electrode using silver adhesive. The completed top and bottom layers were then bonded together using elastic separators to prepare an air gap between the layers and facilitate reciprocal motions of the nanogenerator.

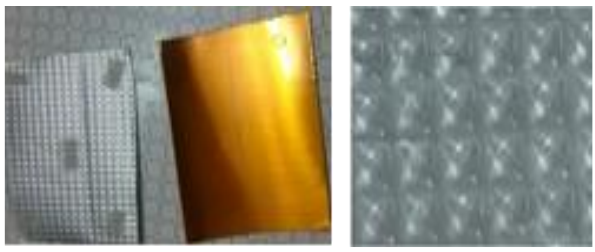


Fig. 2. Image of the pyramidal patterned PDMS layer on Al contact (right) and the upper and bottom layers of TENG with the electrodes and separators (left)

Applied Force and Measurements

To activate the nanogenerator, a reciprocating linear motion mechanism was lab designed and constructed to be used for applying periodic impact forces. The mechanism, illustrated in Fig. 3, was capable of generating linear impact forces with adjustable loads and frequencies tailored to the requirements of the nanogenerator. In this motor, reciprocating linear motion is generated using the repulsive and attractive forces between two magnets. To regulate the speed of movement, a potentiometer is placed in the path of the incoming current to the coil of the temporary magnet. The applied force was measured using a load cell with an accuracy of 1%. By adjusting the resistance of the potentiometer, the frequency of the impact motions is controlled. The linear motor operates within a frequency range of 1–20 Hz, with an applied force of 20 mN.

The nanogenerator's output voltage and current were subsequently measured using an auto-range dual-channel multimeter (GDM-8261), offering a resolution of 0.1 to 10 μV for voltage ranges of 100 mV and 10 V, and 0.1 to 1 nA for current ranges of 100 μA and 1 mA, respectively.

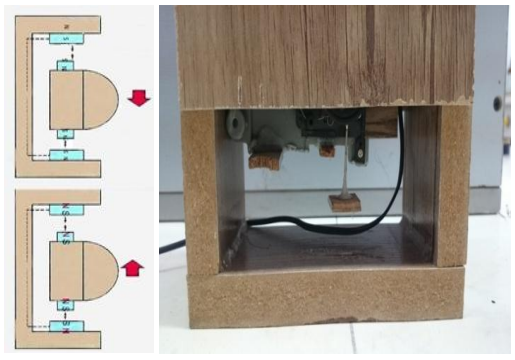


Fig. 3. Schema and photo of the reciprocating linear moving machine for generating impact periodic forces

Mathematical Formulation and Modeling Procedure

The behavior of TENG under the periodic impact force was assumed to be uniform (X_1=X_2=X_3) and one-dimensional as shown in Fig. 4.

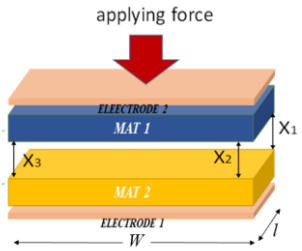


Fig. 4. Schema representing separated TENG layers and the direction of the loading force

The charge transfer in the nanogenerator is exclusively facilitated through an external circuit, ensuring that the two electrodes of the TENG are thoroughly insulated to prevent any leakage currents. When the top and bottom parts of the device are contacted by the applied force, the triboelectric charges are transferred between the surfaces (denoted as Q). Therefore the equal charges are induced on the metallic electrodes and contributes to the generation of electrical potential at the output. As illustrated in Eq. 1 [16], the electrical potential generated by the TENG comprises two components. The first component, $V_{oc}(x)$ (open circuit voltage), originates from the polarized triboelectric charges. The second component arises from the intrinsic capacitive behavior of the TENG. Together, these two factors contribute to the total output voltage observed across the external circuit.

$$V = -\frac{1}{C(x)}Q + V_{oc}(x) \quad (1)$$

The corresponding electrical circuit model of TENG is shown in Fig. 5.

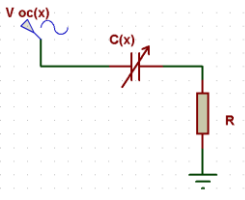


Fig. 5. Equivalent model for TENG with a resistive load

So the Eq.1 can be written as:

$$R\frac{dQ}{dt} = -\frac{1}{C}Q + V_{oc} \quad (2)$$

This first order differential equation is integrated based on the following conditions [20]:

At t=0 and t=T; Q=0, where T is period of actuating forces.

$$Q(t) = \frac{1}{R}e^{-\frac{1}{R}\int_0^t \frac{1}{C(x(t))}dt}\int_0^t V_{oc}\,(x(t))e^{\frac{1}{R}\int_0^t\left(\frac{1}{C(x(t))}dt\right)}dt \quad (3)$$

$$I(t) = \frac{V_{oc}}{R} - \frac{1}{R^2 c}e^{-\frac{1}{R}\int_0^t \frac{1}{C(x(t))}dt}\int_0^t V_{oc}\,(x(t))e^{\frac{1}{R}\int_0^t\left(\frac{1}{C(x(t))}dt\right)}dt \quad (4)$$

$$V(t) = V_{oc} - \frac{1}{RC}e^{-\frac{1}{R}\int_0^t \frac{1}{C(x(t))}dt}\int_0^t V_{oc}\,(x(t))e^{\frac{1}{R}\int_0^t\left(\frac{1}{C(x(t))}dt\right)}dt \quad (5)$$

The equations governing the system depend on the distance (x) between the two electrodes. In the initial approach, it is assumed that this distance remains uniform across the entire electrode surfaces and that the electrodes remain parallel under the influence of external forces, However, in practice, the applied forces are often non-uniform, leading to variations in the distance between the electrodes, at the corner of the device.

As a result, the original model for calculating the triboelectric capacitance must be refined. By accounting for the edge effect, the triboelectric capacitance can be accurately modified, as expressed in [21].

$$C_{total} = C_{pp} + C_{fringe} = \frac{w\varepsilon_{ri}}{d_i} + \frac{2\pi\varepsilon_{ri}}{\log\left(\frac{d_i}{H}\right)} \quad (6)$$

In the capacitor model for TENG, H represents the metal thickness, W denotes the width of the device, ε_{ri} is the relative coefficient of dielectric layer, di signifies the thickness of the dielectric layer, and w is defined as w=W−H/2. Utilizing the dielectric-to-dielectric contact mode model (metal/KAPTON/PDMS/metal) for the triboelectric nanogenerator, the corresponding capacitance diagram for this structure is illustrated in Fig. 6.

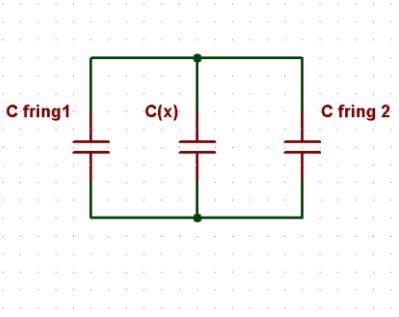


Fig. 6. Capacitive Triboelectronic Nanogenerator Diagram

In Fig. 6, C(x) represents the variable capacitance influenced by the air gap distance, while the capacitors C fring1(x) and C fring2(x) denote the edge-effect capacitors resulted from curvature form of the edge. Based on this configuration, the capacitance value utilized in Equations 3 and 4 should be substituted with the expression outlined in Equation 7, where S is the area of the device (w×l).

$$C_{total}(x) = \frac{\varepsilon_0 S}{\frac{d_1}{\varepsilon_{r1}} + \frac{d_2}{\varepsilon_{r2}}} + \frac{2\pi\varepsilon_{r1}}{\log\left(\frac{d_1}{H}\right)} + \frac{2\pi\varepsilon_{r2}}{\log\left(\frac{d_2}{H}\right)} \quad (7)$$

Simulation results based on the modified capacitance value are referred to as modified simulation results in Section 4.3 and subsequent sections.

These equations were solved numerically using the following flowchart shown in Fig. 7.

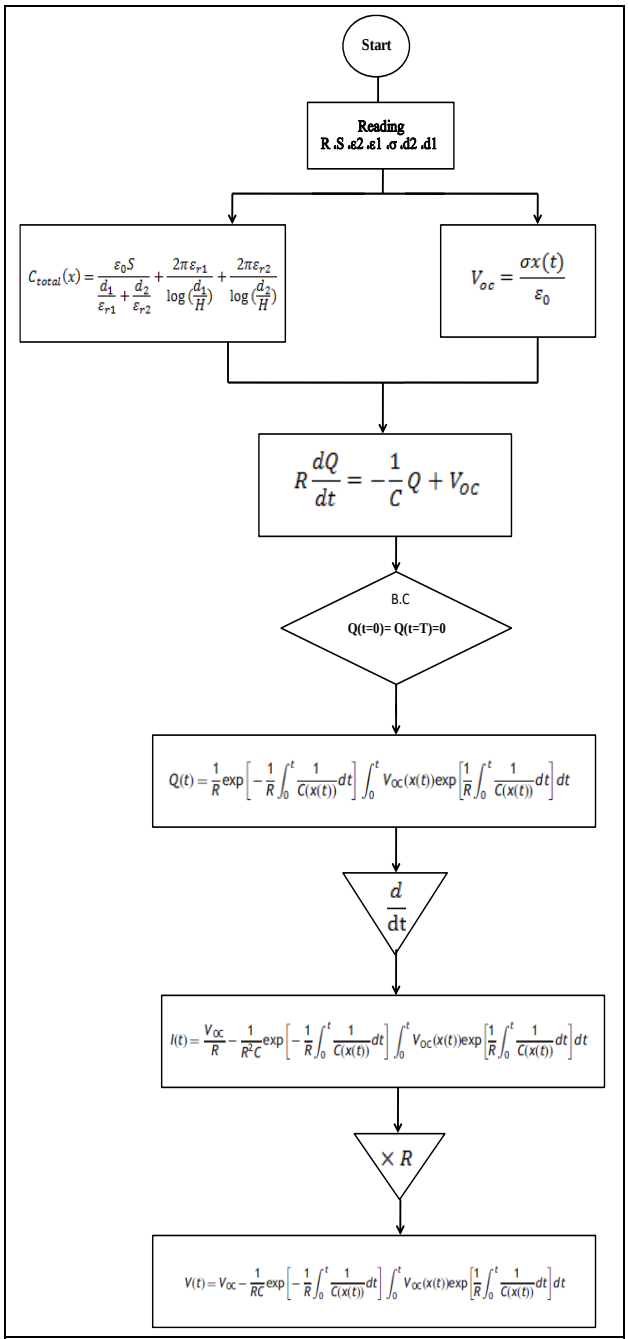


Fig. 7. Flowchart of the modeling procedure for TENG

RESULT AND DISCUSSION

Compared Experimental and Simulation Results

To evaluate the performance of the nanogenerators, forces with a frequency of 8 Hz were applied to the top surface of the nanogenerator using the linear reciprocating machine. The resulting outputs, including voltage and current, were measured and analyzed. Figures 8 and 9 present a comparison between the experimental data and the outputs obtained from conventional simulations.

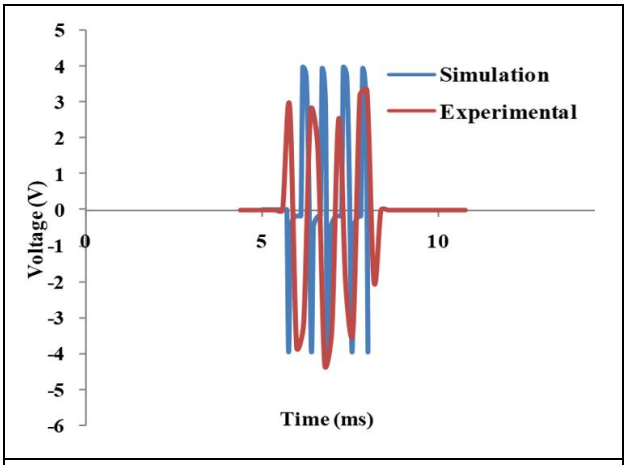


Fig. 8. KAPTON-PDMS Nanogenerator output voltage from the experimental sample and conventional simulation result

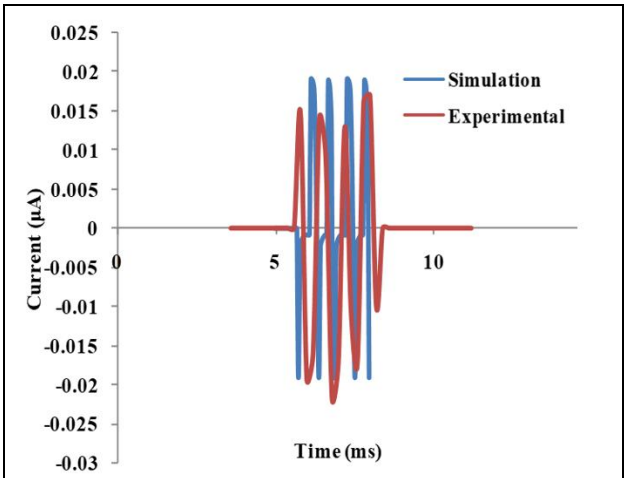


Fig. 9. KAPTON-PDMS Nanogenerator output current from the fabricated sample and conventional simulation result

Applying forces to the top surface of the nanogenerator results in deflection of the PDMS and KAPTON layers, causing them to slide over each other with specific frictional interactions. These interactions facilitate charge transfer between the two dielectric layers, inducing an equal number of opposite charges on the electrodes and generating an electrical potential between them. The fabricated nanogenerator demonstrated strong responsiveness to the applied forces and their frequencies, achieving a maximum output of approximately 3V and a current of 0.02 μA. The rate of charge accumulation on the electrodes is presented in Fig. 10.

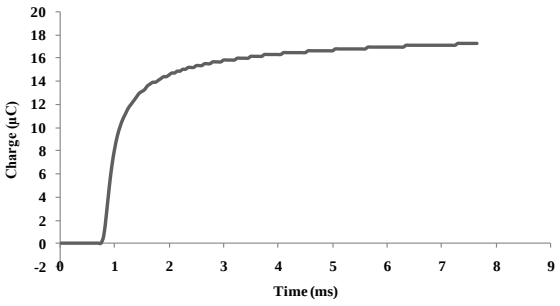


Fig. 10. Charges rate on the PDMS-KAPTON nanogenerator electrodes

Upon the initiation of external forces, the charges on the electrodes rapidly increase and swiftly reach their maximum value. For this nanogenerator, the maximum stored electric charge on the electrodes is approximately 18 µC, resulting from the electron transfer between the two polymer dielectric layers.

The application of external forces causes periodic charging and discharging of the electrodes, corresponding to the frequency of the applied forces.

Effect of The Induced Electrical Charges Rate and The Air gap on the TENG Capacitance

Understanding the responses of the nanogenerator to key design parameters is essential for optimizing its performance. This section examines the effects of the electric charging rate of the capacitance, the air gap between the electrodes, and the corresponding equivalent capacitance through numerical analysis.

Figure 11 illustrates the rate of capacitance change generated between the KAPTON and PDMS layers. It is observed that, under continuous application of forces, the electrodes move closer to each other, thereby reducing the air gap. Initially, the system exhibits a capacitive value of 4.5 nF; however, as the electrodes are forced closer together, the capacitive value gradually decreases. When the air gap between the plates reaches zero, the capacitance change stabilizes accordingly.

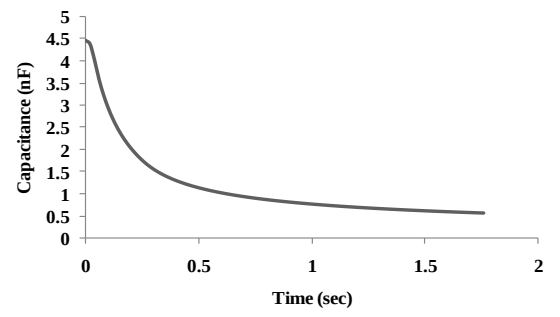


Fig. 11. Rate of the capacitance changing between the plates

Figure 12 illustrates the variation in induced charge on the electrodes of the triboelectric nanogenerator as a function of air gap changes. It can be observed that, as the air gap increases from 0 to 12 mm, the induced charge rises from zero to 10 nC. This behavior indicates that the nanogenerator plates detach after contact, storing electrical charges on the plates. With each cycle of recurrence, the induced electric charge is discharged as electrical current through the connected resistive load.

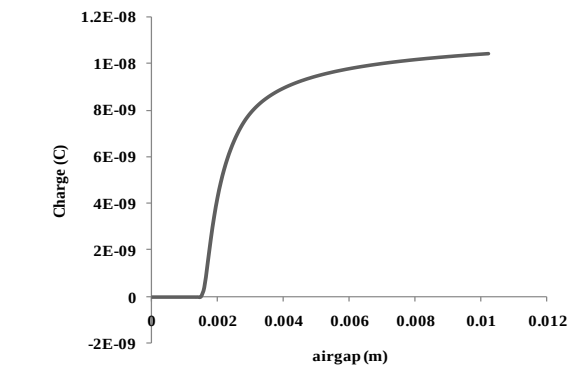


Fig. 12. The induced charge on the electrodes of TENG versus air gap variation

As shown in Figure 13, an increase in air gap reduces the capacitance between the plates. The increase in distance from 0 to 10 mm makes the capacitance change from 0.45nF to 0.05nF.

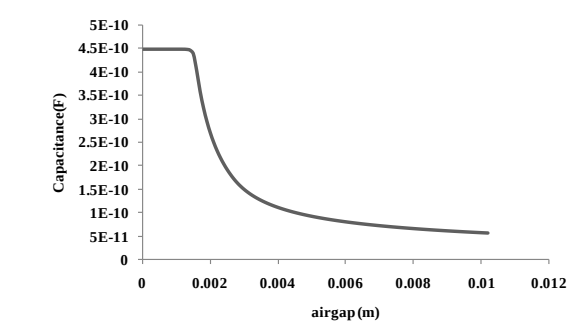


Fig. 13. Capacitance changing versus air gap variations

Other studies have demonstrated a significant relationship between induced charge and changes in capacitive capacitance. As illustrated in Fig. 14, an increase in capacitance corresponds to a reduction in the amount of stored charge on the plates.

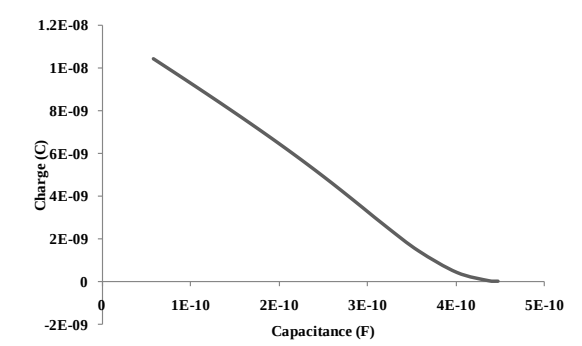


Fig. 14. Induced electrical charges on the electrodes as the TENG capacitance is changing

As a general conclusion from Figs 11 to 14, it can be inferred that the consideration of the air gap between the plates leads to a decrease in capacitance. This reduction in capacitance results in a higher induced charge and improved outflow current. In the present study, the air gap was set at approximately 3 mm due to production constraints, yielding an output current of around 0.015 mA.

Compared Experimental and Modified Simulation Results

A re-simulation incorporating the effect of the new capacitor configuration was conducted, yielding refined results. The outcomes of this re-simulation, based on the corrected capacitive relations, are presented in Fig. 15.

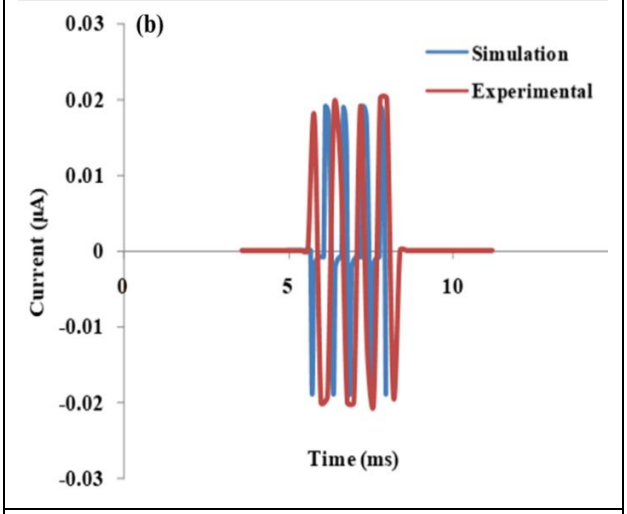


Fig. 15. Voltage and current waveforms taking into account the effect of the edge. a) Voltage b) Flow

It is evident that the diagrams, corrected to account for the edge effect on capacitance, exhibit improved accuracy compared to the voltage and current diagrams presented in figures 8 and 9. The modified diagrams show a closer alignment between the simulation results and the experimental data obtained from laboratory measurements.

As observed, discrepancies remain between the measured and calculated current and voltage signals, particularly in their timing and amplitude. In the simulation, the input force was assumed to be uniformly distributed across the entire device surface, resulting in a vertically uniform displacement. However, in the experiment, the impact force was applied to the device via a small plastic square connected to a rod. Consequently, the force was not distributed uniformly across the entire surface, leading to performance deviations in real measurements.

Additionally, during the experiment, the device beneath the rod experienced unintended movement, introducing further non-uniformity in displacement. This contributed to discrepancies between the measured results and the theoretical calculations.

Furthermore, although the applied section of the motion simulator was intentionally kept small to minimize the inertial effects of its components, the instrument still possessed inertia, which influenced the timing of force application and removal. This inertia was not accounted for in the simulation, where the applied force was expected to activate and deactivate almost instantaneously. This rapid switching also affects charge transfer and induction to the electrode due to the intrinsic capacitance of the device. As a result, a phase shift emerged between the experimental and theoretical results.

Effect of Environmental Conditions on the TENG Output Voltage

The triboelectric nanogenerator exhibits sensitivity to environmental conditions such as air pressure and temperature variations, which influence its performance. The triboelectric principle encompasses two main mechanisms: electron displacement and ion displacement effects. The displacement of electrons depends on the interaction between the polymer and the metal electrode, which is influenced by the work function of the metal electrode [20]. Additionally, wet layers on the polymer surface can significantly affect ion displacement [22–23].

Changes in air pressure also play a role in altering the number of residual charges on the polymer surfaces. Experimental observations [24] reveal that surface charges remain stationary at pressures up to 1 μTorr between polymer and metal, and at pressures of 5 Torr for superfluid conditions. These findings suggest that atmospheric pressure and varying temperature conditions can regulate charge displacement.

As depicted in Fig. 16, an increase in ambient pressure from 200 to 600 Torr enhances the voltage response of the triboelectric nanogenerator. Conversely, as shown in Fig. 17, temperature elevation negatively impacts the nanogenerator's response; increasing the temperature from 25°C to 70°C results in a voltage reduction from 3.5 volts to 1 volt. It is noteworthy that the test conditions and nanogenerator parameters align with those provided in Tables 1 and 2.

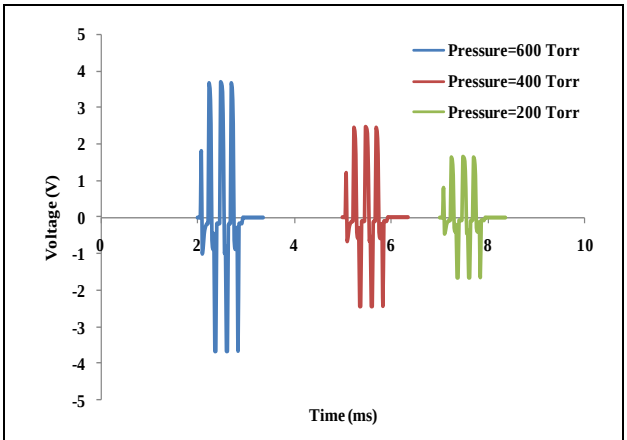


Fig. 16. Survey of environmental air pressure change on triboelectric nanogenerator response

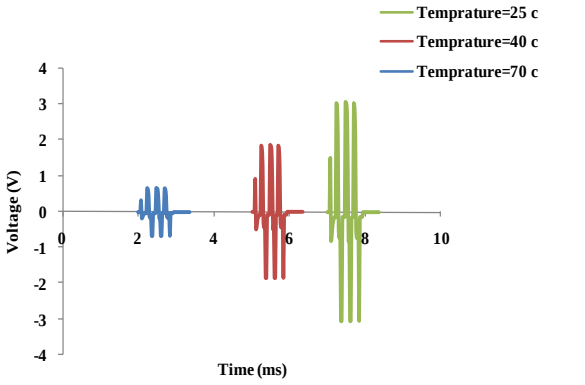


Fig. 17. Checking the ambient air temperature change on triboelectric nanogenerator response

CONCLUSION

In this study, a polymeric triboelectric nanogenerator utilizing KAPTON and PDMS was fabricated and analyzed numerically. To improve result accuracy, the model was refined by incorporating the effects of edge capacitors. A comparison between the experimental data and the proposed model demonstrated improved agreement between the output current and voltage of the nanogenerator.

The fabricated device produced a voltage of approximately 4 V and a current of 0.025 μA when actuated by mechanical vibrations. The influence of various structural parameters was examined through numerical analysis. It was observed that the air gap between the two triboelectric layers significantly affected the generation of electric charge on the plates. Additionally, reducing the thickness of the triboelectric materials increased the nanogenerator's output voltage.

Notably, environmental conditions (pressure and temperature) had a pronounced impact on the nanogenerator's performance, highlighting the sensitivity of the device to changes in its operational surroundings.

REFERENCE

[1] Dresselhaus MS, Thomas IL. Alternative energy technologies. Nature. 2001 Nov;414(6861):332–7.

[2] Kolar, James L. Alternative energy technologies. Environmental Quality Management. 2000;10:45-54.

[3] Xu C, Wang ZL. Compact hybrid cell based on a convoluted nanowire structure for harvesting solar and mechanical energy. Advanced Materials. 2011;23(7):873-877.

[4] Wang ZL, Song J. Piezoelectric nanogenerators based on zinc oxide nanowire arrays. Science. 2006;312(5771):242-6.

[5] Wang S, Lin L, Wang ZL. Nanoscale Triboelectric-Effect-Enabled Energy Conversion for Sustainably Powering Portable Electronics. Nano Letters. 2012;12(12):6339–46.

[6] Fan FR, Tian ZQ, Lin Wang Z. Flexible triboelectric generator. Nano Energy. 2012;1(2):328–34.

[7] Niu H, Du X, Zhao S, Yuan Z, Zhang X, Cao R, et al. Polymer nanocomposite-enabled high-performance triboelectric nanogenerator with self-healing capability. RSC Adv. 2018;8(54):30661–8.

[8] Mule AR, Dudem B, Patnam H, Graham SA, Yu JS. Wearable single-electrode-mode triboelectric nanogenerator via conductive polymer-coated textiles for self-power electronics. ACS Sustain Chem Eng. 2019;7(19):16450–8.

[9] Shao J, Willatzen M, Wang ZL. Theoretical modeling of triboelectric nanogenerators (TENGs). J Appl Phys. 2020;128(11).

[10] Chen H, Lu Q, Cao X, Wang N, Wang ZL. Natural polymers based triboelectric nanogenerator for harvesting biomechanical energy and monitoring human motion. Nano Res. 2022;15(3):2505–11.

[11] Heydari M, Sheikholeslami TF, Behzadmehr A. Design and optimization of a spiral electrode triboelectric nanogenerator using response surface methodology. Adv Electr Electron Eng. 2022;20(2).

[12] Heydari MA, Fanaei S T, Behzadmehr A. Design and fabrication of a spiral electrode triboelectric nanogenerator and application as zero power dynamic sensor. FME Trans. 2022;50(2):294–301.

[13] Shao J, Willatzen M, Wang ZL. Theoretical modeling of triboelectric nanogenerators (TENGs). Journal of Applied Physics. 2020;128(11):111101.

[14] Sun B, Guo X, Zhang Y, Wang ZL, Shao J. A generalized model for a triboelectric nanogenerator energy harvesting system. Nano Energy. 2024;126(109637):109637.

[15] Zhao H, Wang H, Yu H, Xu Q, Li X, Guo J, et al. Theoretical modeling of contact-separation mode triboelectric nanogenerators from initial charge distribution. Energy Environ Sci. 2024;17, 2228-2247.

[16] Niu S, Wang S, Lin L, Liu Y, Zhou YS, Hu Y, et al. Theoretical study of contact-mode triboelectric nanogenerators as an effective power source. Energy & Environmental Science. 2013;6(12):3576-83.

[17] Niu S, Zhou YS, Wang S, Liu Y, Lin L, Bando Y, et al. Simulation method for optimizing the performance of an integrated triboelectric nanogenerator energy harvesting system. Nano Energy. 2014;8:150-6.

[18] Wang S, Xie Y, Niu S, Lin L, Liu C, Zhou YS, et al. Maximum Surface Charge Density for Triboelectric Nanogenerators Achieved by Ionized-Air Injection: Methodology and Theoretical Understanding. Advanced Materials. 2014;26(39):6720-8.

[19] Miranda I, Souza A, Sousa P, Ribeiro J, Castanheira EMS, Lima R, Minas G. Properties and Applications of PDMS for Biomedical Engineering: A Review. Journal of Functional Biomaterials. 2022; 13(1):2.

[20] Lowell J. The electrification of polymers by metals. Journal of Physics D: Applied Physics. 1976;9(11):1571.

[21]. Rabaey JM, Chandrakasan AP, Nikolic B. Digital integrated circuits: Prentice hall Englewood Cliffs; 2002.

[22] Pence S, Novotny V, Diaz A. Effect of surface moisture on contact charge of polymers containing ions. Langmuir. 1994;10(2):592-6.
[23] Wiles JA, Fialkowski M, Radowski MR, Whitesides GM, Grzybowski BA. Effects of surface modification and moisture on the rates of charge transfer between metals and organic materials. The Journal of Physical Chemistry B. 2004;108(52):20296-302.
[24] McCarty LS, Whitesides GM. Electrostatic charging due to separation of ions at interfaces: contact electrification of ionic electrets. Angewandte Chemie International Edition. 2008;47(12):2188-207.